



1 **Glaciers determine the sensitivity of hydrological processes to perturbed climate**
2 **in a large mountainous basin on the Tibetan Plateau**

3
4 **Yi Nan ¹, Fuqiang Tian ¹**

5 **Affiliation:**

6 1. State Key Laboratory of Hydrosience and Engineering & Department of Hydraulic
7 Engineering, Tsinghua University, Beijing 100084, China

8
9 **Corresponding to:** Fuqiang Tian

10 Email: tianfq@tsinghua.edu.cn

11
12 **Abstract**

13 The major rivers on the Tibetan Plateau supply important freshwater resources to riparian
14 regions, but are undergoing significant climate change in recent decades. Understanding the
15 sensitivities of hydrological processes to climate change is important for water resource
16 management, but large divergences existed in previous studies because of the uncertainties of
17 hydrological models and climate projection data. Meanwhile, the spatial pattern of local
18 hydrological sensitivities was poorly explored despite the strong heterogeneity on the Tibetan
19 Plateau. This study adopted the climate perturbation method to analyze the hydrological
20 sensitivities of a typical large mountainous basin (Yarlung Tsangpo River, YTR) to climate
21 change. We utilized the tracer-aided hydrological model Tsinghua Representative Elementary
22 Watershed-Tracer-aided version (THREW-T) to simulate the hydrological and cryospheric
23 processes in the YTR basin. Datasets of multiple objectives and internal stations were used to
24 validate the model, to provide confidence to the baseline simulation and the sensitivity analysis.
25 Results indicated that: (1) The THREW-T model performed well on simulating the streamflow,
26 snow cover area (SCA), glacier mass balance (GMB), and stream water isotope, ensuring good
27 representation of the key cryospheric processes and a reasonable estimation of runoff
28 components. The model performed acceptably on simulating the streamflow at eight internal
29 stations located in the mainstream and two major tributaries, indicating that the spatial pattern



30 of hydrological processes was reflected by the model. (2) Increasing temperature led to
31 decreasing annual runoff, smaller inter-annual variation, more even intra-annual distribution,
32 and an earlier maximum runoff. It also influenced the runoff regime by increasing the
33 contributions of rainfall and glacier melt overland runoff, but decreasing the subsurface runoff
34 and snowmelt overland runoff. Increasing precipitation had the opposite effect to increasing
35 temperature. (3) The local runoff change in response to increasing temperature varied
36 significantly, with changing rate of -18.6% to 54.3% for 5°C of warming. The glacier area ratio
37 (GAR) was the dominant factor of the spatial pattern of hydrological sensitivities to both
38 perturbed temperature and precipitation. Some regions had a non-monotonic runoff change rate
39 in response to increasing temperature, the GAR and mean annual precipitation (MAP) of which
40 showed linear relation, and formed the boundary of regions with different trends in response to
41 climate warming in the GAR-MAP plot.
42



43 1. Introduction

44 The Tibetan Plateau (TP), known as the “Asian Water Tower”, is the source region of
45 several major rivers in Asia (e.g., Yarlung Tsangpo-Brahmaputra Lantsang-Mekong, Indus,
46 Ganges). The contributions of runoff in the source regions of TP rivers to the total runoff in
47 whole basins range from 6%-60% (Tang et al., 2019; Wang et al., 2020; Cao and Pan, 2014),
48 sustaining the ecosystems and supplying valuable freshwater resources for downstream
49 livelihoods (Immerzeel et al., 2010; Lutz et al., 2014). The sustainable socioeconomic
50 development and the decision-making of water resource management in the riparian countries
51 around the TP rely heavily on the runoff in the major river basins (Cui et al., 2023). Meanwhile,
52 the TP is a typical high mountainous cryosphere, characterized by large stores of frozen soil
53 and frequent multiphase water transferring, resulting in complex hydrological processes and
54 multiple water sources including rainfall, snowmelt and glacier melt (Li et al., 2019; Yao et al.,
55 2022). The melting processes of frozen water are determined by temperature, and the runoff
56 change on the TP is extremely sensitive to climate change (Gao et al., 2019). Consequently,
57 understanding hydrological processes and estimating the runoff change on the TP is not only of
58 great practical significance, but also a frontier scientific question in global change.

59 The TP is undergoing significant climate change in recent decades, with a warming rate
60 twice the global average level (Yao, 2019). Based on the recently released Coupled Model
61 Intercomparison Project Phase 6 (CMIP6) (Eyring et al., 2016), the warming levels of 1.5°C,
62 2°C and 3°C over the TP will be attained around the 2030s, 2050s and 2070s, respectively, and
63 the precipitation is also likely to increase significantly (Cui et al., 2023). The hydrological
64 cycling and water resources will change correspondingly; thus it is important to understand the
65 hydrological processes on the TP and the hydrological response to climate change. Plenty of
66 studies have adopted hydrological models to project the runoff change on the TP in the future,
67 but the reported trends and changing rates varied considerably in existing studies. Wang et al.
68 (2021) and Lutz et al. (2014) projected an increasing runoff trend till the end of 21st century,
69 while Cui et al. (2023) predicted the runoff to decrease before the 2030s and turn over to an
70 increasing trend after that. A primary reason for the divergence in existing studies is the model
71 uncertainties. The parameters are usually inadequately constrained solely by the streamflow
72 observation data because of the complex hydrological processes, resulting in large uncertainties



73 in the estimation on the contributions of runoff components (Tian et al., 2020; Nan et al., 2021a),
74 which influence the runoff projection significantly. For instance, Lutz et al. (2014) estimated
75 the contribution of glacier melt to annual runoff as 0.86-40.59% in the major TP rivers, resulting
76 in an increasing runoff with climate warming, while Cui et al. (2023) estimated the contribution
77 as 0.73-14.33% and resulting in a decreasing trend in the near future. Nonetheless, recently
78 developed hydrological models integrating key cryospheric processes (e.g., Cui et al., 2023)
79 have been proved as effective tools for hydrological simulations on the TP, and the high-quality
80 datasets of snow and glacier (e.g., Chen et al., 2018; Hugonnet et al., 2022) can provide
81 adequate validation for the corresponding processes. Moreover, tracer-aided hydrological
82 models integrating modules of tracer storage, mixture, and transportation processes forced by
83 the outputs of isotopic general circulation models (iGCMs) have proved to constrain the
84 hydrological model uncertainties significantly (He et al., 2019; Birkel and Soulsby, 2015;
85 Stadnyk and Holmes, 2023), especially for the separation of runoff components (Nan et al.,
86 2021a, 2023). These developments of models and datasets bear the potential to provide a more
87 reasonable baseline for streamflow projection.

88 Another major source of runoff projection uncertainty is the uncertainty of climatic forcing
89 data (Li et al., 2014). The climatic data in the future are generally generated by the general
90 circulation models (GCMs), which cannot be directly adopted in the catchment scale because
91 of the insufficient spatial resolution and accuracy, so downscaling and bias correction are
92 necessary steps in using GCM data at regional scale (Xu et al., 2019; Olsson et al., 2015).
93 However, even being corrected by the observation data during the historical period, the
94 divergence among the outputs of different GCMs is still significant. For example, the difference
95 in the precipitation change over the TP among 22 CMIP6 products could be larger than 50%
96 (Cui et al., 2023). Bloschl and Montanari (2010) pointed out the large uncertainties of studies
97 analyzing the impact of climate change, and likened them to throwing a dice. As an alternative
98 method, producing hypothesized climate change scenarios by perturbing the current
99 temperature and precipitation data has proved to be valuable in investigating the hydrological
100 sensitivities to climate change (Ayguen et al., 2020; Rasouli et al., 2015; He et al., 2021b). The
101 range of climate perturbation is assumed based on the possible change range projected by an
102 ensemble of GCMs, providing a possible runoff change range accordingly (Su et al., 2023; He



103 et al., 2021b). The climate perturbation method also allows for a deeper analysis of the separate
104 effect of each climatic factor and the compensation effects among them (He and Pomeroy,
105 2023).

106 Although plenty of studies have been conducted for the TP rivers to project the runoff
107 change or analyze the hydrological sensitivities to climate change, most of them were
108 conducted at the regional or basin scale (e.g., Su et al., 2023; Zhang et al., 2022). The local
109 hydrological response to climate change could significantly differ among small catchments due
110 to the different geographical and meteorological characteristics (Bai et al., 2023), which is
111 important for local water resources utilization and management (Zhang et al., 2015).
112 Considering the strong heterogeneity in meteorological factors and land surface conditions in
113 the large river basins on the TP (Wang et al., 2021; Li et al., 2020), the local hydrological
114 sensitivities to climate change should have strong variability over the TP. However, the spatial
115 pattern and influence factors of the local hydrological sensitivities within the basin are poorly
116 explored, partly due to the scarce hydrological stations for model validation, resulting in a lack
117 of confidence in the spatial representation of hydrological processes.

118 Motivated by the mentioned background, this study utilized the spatially distributed tracer-
119 aided hydrological model THREW-T developed by Nan et al. (2021b) in the Yarlung Tsangpo
120 River basin, a typical large mountainous basin on the Tibetan Plateau, to explore its
121 hydrological sensitivity to perturbed temperature and precipitation. Snow, glacier, and isotope
122 data and observation streamflow at nine stations were collected to validate the model. The
123 spatial pattern of the local hydrological sensitivities and the influence factors were analyzed in
124 particular. The main objectives of this study are as follows: (1) to test the performance of
125 THREW-T model on simulating all the hydrological and cryospheric processes in the Yarlung
126 Tsangpo River basin, (2) to analyze the sensitivities of hydrological processes in the Yarlung
127 Tsangpo River basin to a reasonable range of perturbed temperature and precipitation, and (3)
128 to analyze the spatial pattern and the influence factors of the local hydrological sensitivities.

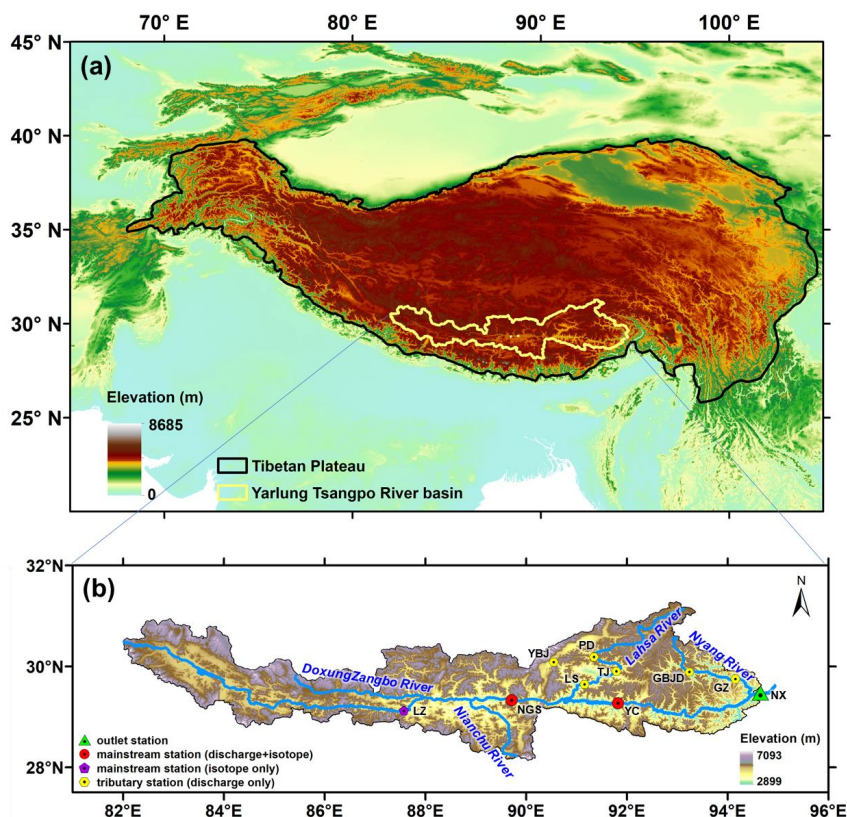
129 **2. Data and methodology**

130 **2.1 Study area**

131 This study focused on the Yarlung Tsangpo River (YTR) basin, the upstream part of the



132 Brahmaputra River basin, located in the southern TP (Figure 1). The YTR is one of the longest
133 rivers originating from the TP (longer than 2000 km), extending in the range of 27-32°N and
134 82-97°E with an elevation extent of 2900-6900 m a.s.l. (above sea level). The mean annual
135 precipitation and temperature in the YTR basin are around 500 mm and -0.2 °C, respectively.
136 The YTR has four major tributaries, i.e., DoxungZangbo, Nianchu River, Lhasa River, and
137 Nyang River, from upstream to downstream. The precipitation is dominated by the South Asian
138 monsoon in the Indian Ocean hydrosphere-atmosphere system, resulting in an obviously wet
139 season from June to September. The outlet hydrological station along the mainstream is the
140 Nuxia station, above which the drainage area is approximately 2×10^5 , and around 1.5% is
141 covered by glaciers.



142
143 **Figure 1.** Locations and topography of (a) the Tibetan Plateau and (b) the Yarlung Tsangpo
144 River basin. The stations used for model validation are shown in Figure (b). The abbreviations



145 NX, YC, NGS, LZ, GZ, GBJD, LS, TJ, PD and YBJ represent Nuxia, Yangcun, Nugesha, Lazi,
146 Gengzhang, Gongbujiangda, Lahsa, Yangjia, Pangduo and Yangbajing stations, respectively.

147 2.2 Data

148 The 30 m resolution digital elevation model (DEM) data for the YTR basin was extracted
149 from the Geospatial Data Cloud (<https://www.gscloud.cn>). Daily precipitation, temperature,
150 and potential evapotranspiration data were extracted from the China Meteorological Forcing
151 Dataset (CMFD, Yang and He, 2019) with 0.1° resolution. For the cryospheric processes, the
152 Tibetan Plateau Snow Cover Extent (TPSCE) product (Chen et al., 2018) and the second glacier
153 inventory dataset of China (Liu, 2012) were adopted to denote the snow and glacier coverage.
154 The yearly glacier elevation change data with 0.5° resolution developed by Hugonnet et al.
155 (2021) was used to represent the glacier mass balance. For the underlying conditions, the
156 MODIS leaf area index (LAI) product MOD15A2H (Myneni et al., 2015) and normalized
157 difference vegetation index (NDVI) product MOD13A3 (Didan, 2015) were adopted to
158 represent the vegetation coverages, and the Harmonized World Soil Database (HWSD, He,
159 2019) was used to estimate the soil property parameters. Daily streamflow data at nine stations
160 were collected (Figure 1 and Table 1).

161 **Table 1.** The name, location and data period of the hydrological stations

Station	Mainstream/tributary	Period
Nuxia	Mainstream	2001-2015
Yangcun	Mainstream	2001-2010
Nugesha	Mainstream	2001-2010
Gengzhang	Nyang river	2001-2015
Lhasa	Lhasa river	2001-2015
Gongbujiangda	Nyang river	2006-2009, wet season
Yangbajing	Lhasa river	2006-2015, wet season
Pangduo	Lhasa river	2001-2015, wet season
Tangjia	Lhasa river	2001-2015, wet season

162 Grab samples of precipitation and stream water were collected in 2005 at four stations
163 along the mainstream of YTR, i.e., Lazi, Nugesha, Yangcun, and Nuxia, from upstream to
164 downstream, for isotope analysis (Table 2, Liu et al., 2007). The outputs of Scripps Global
165 Spectral Model with isotope incorporated (isoGSM, Yoshimura et al., 2008) with 1.875°
166 resolution were extracted to represent the spatiotemporal variation of precipitation isotope in
167 the YTR basin. According to our previous assessment based on the measurement precipitation



168 isotope data, the isoGSM captured the seasonality of precipitation isotope well, but had
169 systematic overestimation biases in the YTR basin, which were highly correlated to the altitude
170 (Nan et al., 2021a). The corrected isoGSM in the YTR basin produced by Nan et al. (2022) was
171 adopted in this study.

172 **Table 2.** Summary of measurement isotope data in the YTR basin during 2005

Station	Period	Precipitation			Stream		
		Sample number	$\delta^{18}\text{O}$ (‰)	SD (‰)	Sample number	$\delta^{18}\text{O}$ (‰)	SD (‰)
Nuxia	14 Mar. – 23 Oct.	86	-10.33	7.18	34	-15.74	1.60
Yangcun	17 Mar. – 5 Oct.	59	-13.17	7.10	30	-16.57	1.69
Nugesha	14 May. – 22 Oct.	45	-14.29	7.99	25	-17.84	0.99
Lazi	6 Jun. – 22 Sep.	42	-17.41	5.75	22	-16.52	1.43

173 2.3 The tracer-aided hydrological model

174 A distributed tracer-aided hydrological model, Tsinghua Representative Elementary
175 Watershed-Tracer-aided version (THREW-T) model, developed by Tian et al. (2006) and Nan
176 et al. (2021b), was adopted to simulate the hydrological and isotopic processes in the YTR basin.
177 The model uses the representative elementary watershed (REW) method for spatial
178 discretization of basins, dividing the whole catchment into REWs based on DEM data. Each
179 REW is further divided into two vertically distributed layers (i.e., surface and subsurface layers),
180 including eight subzones (i.e., surface layer: vegetation zone, bare zone, main channel reach
181 zone, sub stream network zone, snow-covered zone, and glacier-covered zone; subsurface layer:
182 unsaturated zone and saturated zone) (Reggiani et al., 1999; Tian et al., 2006). This study
183 divided the YTR basin into 297 REWs, with an average area of 694 km², ranging from 162 to
184 2753 km². More model details are provided in Tian et al. (2006).

185 A cryospheric module representing the evolutions of snowpack and glacier was
186 incorporated into the model for application in cold regions. The total precipitation was
187 partitioned into liquid and solid precipitation according to a temperature threshold, which was
188 set as 0°C. The degree-day factor method was used to calculate the meltwater. The snow water
189 equivalent of each REW was updated based on the snowfall (i.e., the solid precipitation) and
190 the snowmelt, and the snow cover area was then determined by the snow cover depletion curve
191 (Fassnacht et al., 2016). To simulate the evolution of glaciers, each REW is further divided into



192 several elevation bands to represent the change in temperature and precipitation along the
193 altitudinal profile. The glacier within the intersection of each REW and elevation band is
194 regarded as the representative unit for glacier simulation, similar to the discretization strategy
195 adopted by Luo et al. (2013). For each glacier simulation unit, the model simulates the processes
196 including the accumulation and melt of snow over glacier, the turnover of snow to ice, and the
197 ice melt. More details and equations of the cryospheric module are provided in Nan et al. (2021b)
198 and Cui et al. (2023).

199 The tracer module was incorporated into the model to simulate the isotope composition of
200 multiple water bodies. The Rayleigh equation was adopted to simulate the isotope fractionation
201 during water evaporation and snowmelt processes (He et al., 2019; Hindshaw et al., 2011). The
202 isotope composition of glacier meltwater was assumed to be constantly more depleted than the
203 local precipitation isotope and was estimated by an offset parameter (Nan et al., 2022). The
204 isotope compositions in each simulation unit were calculated based on the complete mixing
205 assumption. Forced by the precipitation isotope composition, the model can simulate the
206 isotope composition of all water bodies, including stream water, soil water, groundwater, and
207 snowpack. More details and calculation equations of the tracer module are provided in Nan et
208 al. (2021b).

209 The THREW-T model quantified the contributions of multiple runoff components based
210 on the flow-pathway definition as reviewed by He et al. (2021a). The runoff was firstly divided
211 into surface runoff and subsurface runoff (baseflow) based on the runoff generation pathway.
212 The surface runoff was then further divided into three components induced by different water
213 sources (rainfall, snowmelt, and glacier melt). As a result, the total runoff was divided into four
214 components: subsurface runoff, rainfall overland runoff, snowmelt overland runoff, and glacier
215 melt overland runoff.

216 **2.4 Model calibration and evaluation**

217 The model was run for 15 years starting from 2001 to 2015, and was calibrated toward
218 four objectives: the discharge at Nuxia station from 2001 to 2015, the snow cover area (SCA)
219 from 2001 to 2015, the average glacier mass balance (GMB) from 2001 to 2010 in the whole
220 YTR basin, and the stream water isotope at the four stations in 2005. The Nash-Sutcliffe



221 efficiency (NSE) was set as the calibration function for discharge and isotope objectives, and
 222 the root mean square error (RMSE) was set as the calibration for SCA and GMB objectives.
 223 The optimization objective function of calibration procedure was calculated by combining the
 224 function of each objective with equal weights. The physical basis, reference ranges and
 225 calibrated values of the calibrated parameters in the THREW-T model are shown in Table 3.

226 Apart from the calibration functions, the model performances were additionally evaluated
 227 by three statistical metrics: logarithmic NSE (lnNSE), normalized root mean square error
 228 (NRMSE) and correlation coefficient (CC). The discharge simulation was evaluated by lnNSE
 229 to examine the simulation of baseflow process. Discharge data at eight internal stations (Figure
 230 1) were collected to assess the spatial consistency of model performance, and NRMSE metric
 231 was adopted to evaluate the discharge simulation at the stations where only the data during wet
 232 seasons were available (Gongbujiangda, Yangbajing, Pangduo, and Tangjia stations). The
 233 RMSE and CC of the cumulative glacier mass balance since the beginning of simulation period
 234 were also calculated to assess the glacier simulation, considering the temporal interpolation
 235 adopted by Hugonnet et al. (2021) which led to uncertainty in the year scale data.

$$236 \quad \text{NSE} = 1 - \frac{\sum(X_o - X_s)^2}{\sum(X_o - \bar{X}_o)^2} \quad (1)$$

$$237 \quad \text{lnNSE} = 1 - \frac{\sum(\ln(X_o) - \ln(X_s))^2}{\sum(\ln(X_o) - \ln(\bar{X}_o))^2} \quad (2)$$

$$238 \quad \text{RMSE} = \sqrt{\frac{\sum(X_o - X_s)^2}{n}} \quad (3)$$

$$239 \quad \text{NRMSE} = \frac{\text{RMSE}}{\bar{X}_o} \quad (4)$$

$$240 \quad \text{CC} = \frac{\sum[(X_s - \bar{X}_s)(X_o - \bar{X}_o)]}{\sqrt{\sum[(X_s - \bar{X}_s)^2(X_o - \bar{X}_o)^2]}} \quad (5)$$

241 where, X_s , X_o , \bar{X}_s and \bar{X}_o are the simulated, observed, mean of simulated and mean of
 242 observed hydrological variables, respectively, and n is the number of data.

243 **Table 3.** Physical descriptions, reference ranges and calibrated values of the calibrated
 244 parameters in the THREW-T model

Symbol	Unit	Description	Reference range	Calibrated value
WM	cm	Tension water storage capacity used to calculate the saturation area	0-10	2.92
B	-	Shape coefficient used to calculate the	0-1	0.04



		saturation area		
KKA	-	Exponential coefficient to calculate the subsurface runoff outflow rate	0-6	5.92
KKD	-	Linear coefficient to calculate the subsurface runoff outflow rate	0-0.5	0.21
DDF _S	Mm/°C/d	Degree day factor for snowmelt	0-10	2.60
DDF _G	Mm/°C/d	Degree day factor for snowmelt	0-10	1.51
T ₀	°C	Temperature threshold above which snow and glaciers melting occurs	-5 – 5	-4.28
C ₁	-	Coefficient to calculate concentration process using the Muskingum method	0-1	0.04
C ₂	-	Coefficient to calculate concentration process using the Muskingum method	0-1	0.80

245 2.5 Perturbed climatic inputs

246 Daily temperature and precipitation data extracted from the CMFD dataset were set as the
 247 reference climate inputs. Linearly perturbed temperature and precipitation time series were
 248 adopted to represent the potential climate change ranges. Perturbed temperature input data was
 249 generated by adding one-degree increments to the reference daily temperature. The maximum
 250 temperature increase was set as 5 °C, because the temperature in the YTR basin is projected to
 251 increase at 1°C/20 yrs, and will increase by about 5 °C until the end of this decade (Cui et al.,
 252 2023). The influence of changing temperature on the potential evapotranspiration was estimated
 253 by the regression between the two factors (Eq. 6) which was developed by Van Pelt et al. (2009)
 254 and widely adopted in the projection of potential evapotranspiration (e.g., Xu et al., 2019; Cui
 255 et al., 2023). Perturbed precipitation input data was generated by multiplying the reference daily
 256 precipitation data from 80% to 120% with an increment of 10%, similar to Su et al. (2023)
 257 which analyzed the runoff change of three basins on the TP under hypothesized climate change
 258 scenarios. In total, one reference simulation, five simulations of perturbed temperature and four
 259 simulations of perturbed precipitation were conducted. To focus on the influence of climate
 260 perturbations on the hydrological processes, the changes of underlying conditions such as soil
 261 and vegetation were not considered.

$$262 \quad \text{PET} = [1 - \alpha_0(T - \overline{T}_0)] \cdot \overline{\text{PET}}_0 \quad (6)$$

263 where, \overline{T}_0 and $\overline{\text{PET}}_0$ are the mean daily temperature and potential evapotranspiration in each
 264 REW during the simulation period, respectively. T is the daily temperature generated by the
 265 perturbation method. α_0 is determined by regressing the input daily potential

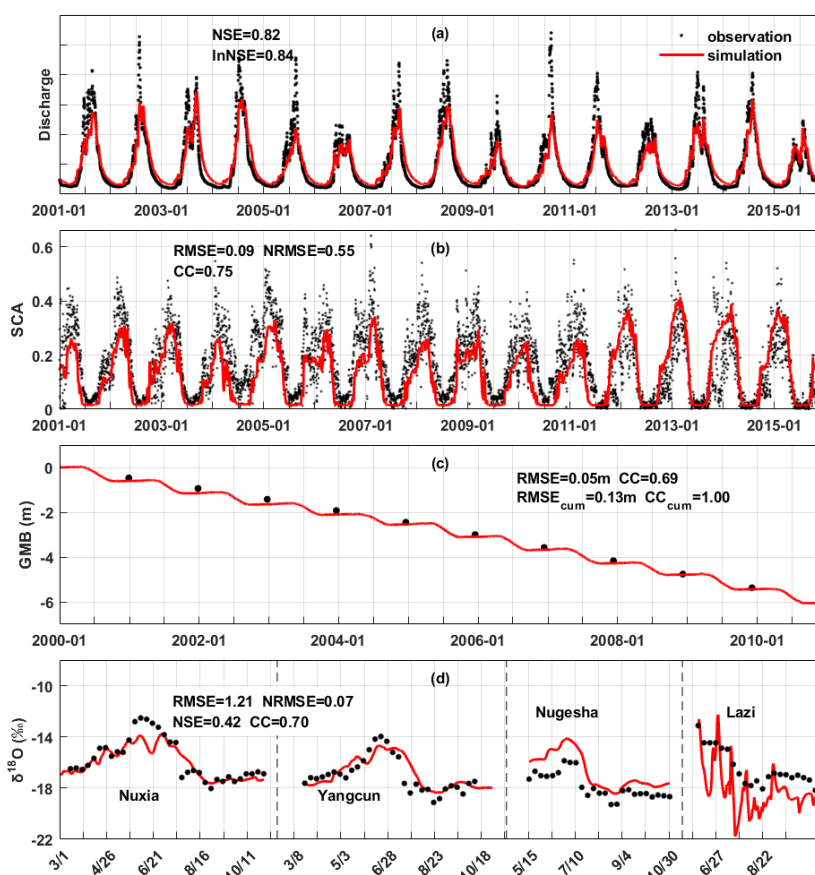


266 evapotranspiration and temperature in each REW.

267 **3. Results**

268 **3.1 Model performance evaluation**

269 Figure 2 shows the model performances on the four calibration objectives. The discharge
270 was simulated well regarding both high flow and baseflow processes, as indicated by the high
271 NSE (0.82) and lnNSE (0.84). The occurring times of peak flow were captured by the model,
272 showing the consistency in the temporal dynamics of simulated and observed streamflow, but
273 the simulated magnitudes of peak flow were slightly lower than the observation (Figure 2a),
274 partly due to the uncertainty of precipitation production (Li et al., 2021). Nonetheless, the
275 simulated annual runoff (302 mm/yr) was very close to the observation (303 mm/yr), indicating
276 that the amount of total runoff was reproduced well. The simulated variation of SCA was
277 smoother than the observation, but the seasonality was captured well, i.e., decreasing sharply
278 in May and remaining extremely low from July to September (Figure 2b). The low RMSE (<0.1)
279 and NRMSE (0.55) suggested that the model performed well on simulating the snow processes.
280 The model successfully simulated the declining glacier (Figure 2c), with an extremely high CC
281 for the cumulative glacier mass balance (~1). The model estimated the annual GMB in the YTR
282 basin as -0.545 m/yr, very close to the value extracted from the dataset of Hugonnet et al. (2021)
283 (-0.554 m/yr). The model simulated the variation of stream isotope well, indicated by the high
284 CC and low NRMSE, which provided confidence in the partitioning among different runoff
285 components (Nan et al., 2021a; He et al., 2019). The seasonality of the isotope was adequately
286 captured: getting enriched in May, reaching maximum in June, and getting depleted in late
287 June/early July (Figure 2d). The fact that the model simultaneously satisfied four calibration
288 objectives ensured the proper representation of the hydrological and cryospheric processes, and
289 provided a reasonable baseline for the sensitivity analysis.

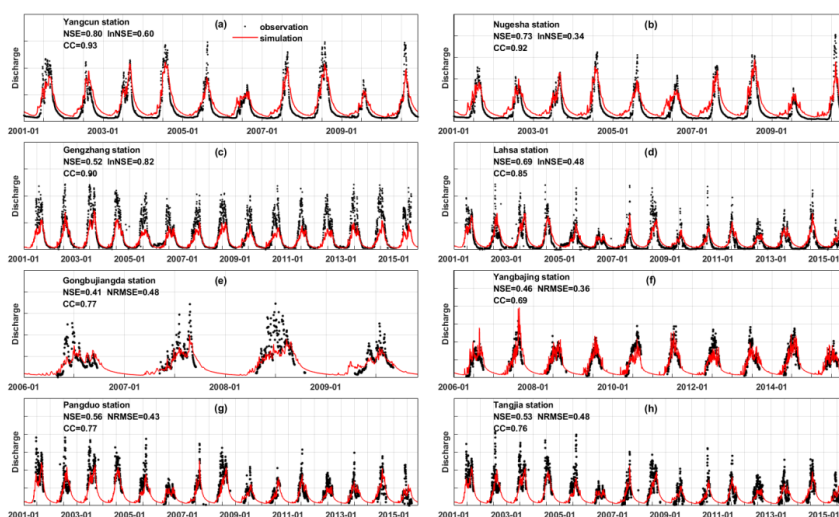


290
291 **Figure 2.** The model performances on the calibration objectives. (a) the streamflow discharge
292 at Nuxia station, (b) the snow cover area ratio in the YTR basin, (c) the average glacier mass
293 balance in the YTR basin, and (d) the stream water isotope at four stations in 2005.

294 Figure 3 shows the streamflow simulation at eight internal stations. At the two stations
295 located along the mainstream (Yangcun and Nugesha), the high flow processes were simulated
296 well as indicated by the high NSE, but the baseflows were overestimated (Figure 3a and b). In
297 contrast, the high flow processes were underestimated at Gengzhang station, but the baseflows
298 were reproduced well (Figure 3c). The model produced fair performance on both high flow and
299 baseflow simulation at Lhasa station, showing moderate NSE and lnNSE (Figure 3d). For the
300 four stations where only the data during the wet season were available, the NRMSEs were all
301 lower than 0.5, indicating that the high flow processes were simulated well (Figure 3e-h).
302 Overall, the streamflow simulations at internal stations were not as good as the calibrated outlet



303 station, but were at acceptable levels. The validation based on the internal stations gave
304 confidence in the spatial pattern of the hydrological processes and their sensitivities to the
305 perturbed climate.



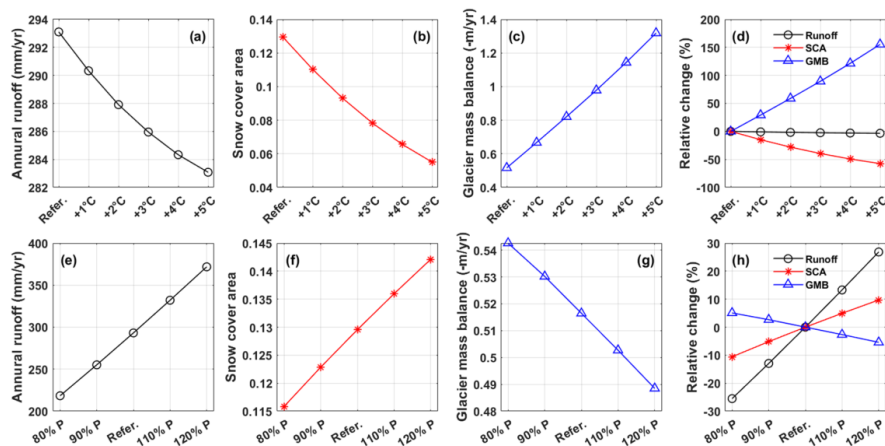
306
307 **Figure 3.** The model performances on the streamflow simulation at the internal stations.

308 3.2 Sensitivities of hydrological variables to perturbed temperature and precipitation

309 The sensitivities of annual runoff, snow cover area, and glacier mass balance to perturbed
310 temperature and precipitation are shown in Figure 4. The relationships between hydrological
311 variables and precipitation/temperature showed strong linearity, which was similar with Su et
312 al. (2023) analyzing the hydrological sensitivities in three other large basins on the TP ($\sim 10^5$
313 km^2), but was different from He et al. (2021b) which conducted a similar analysis in a small
314 boreal forest basin in Canada (603 km^2). The annual runoff kept decreasing with the increasing
315 temperature at the rate of $-2 \text{ mm}/^\circ\text{C}$ due to the increasing evaporation (Figure 4a). The
316 increasing rate got small when the temperature increase was higher than 3°C , partly because
317 the controlling factor of evaporation changed from energy limitation to water limitation (Wang
318 et al., 2022). The snow cover area ratio significantly reduced with the increasing temperature
319 at the rate of $-1.5\%/^\circ\text{C}$ because of the decreasing snowfall and increasing snowmelt, and would
320 be smaller than half of the reference scenario for 5°C of warming (Figure 4b). The glacier mass
321 balance significantly got more negative with the increasing temperature because of the reducing
322 accumulation and increasing meltwater, at the rate of $-0.16 \text{ m}/^\circ\text{C}$ (Figure 4c). Among the three



323 variables, the glacier mass balance was the most sensitive to the warming climate, the relative
 324 change of which could be 150% for 5°C of warming (Figure 4d).



325 **Figure 4.** The sensitivities of annual runoff, snow cover area, and glacier mass balance to the
 326 perturbed temperature (a-d) and precipitation (e-g).
 327

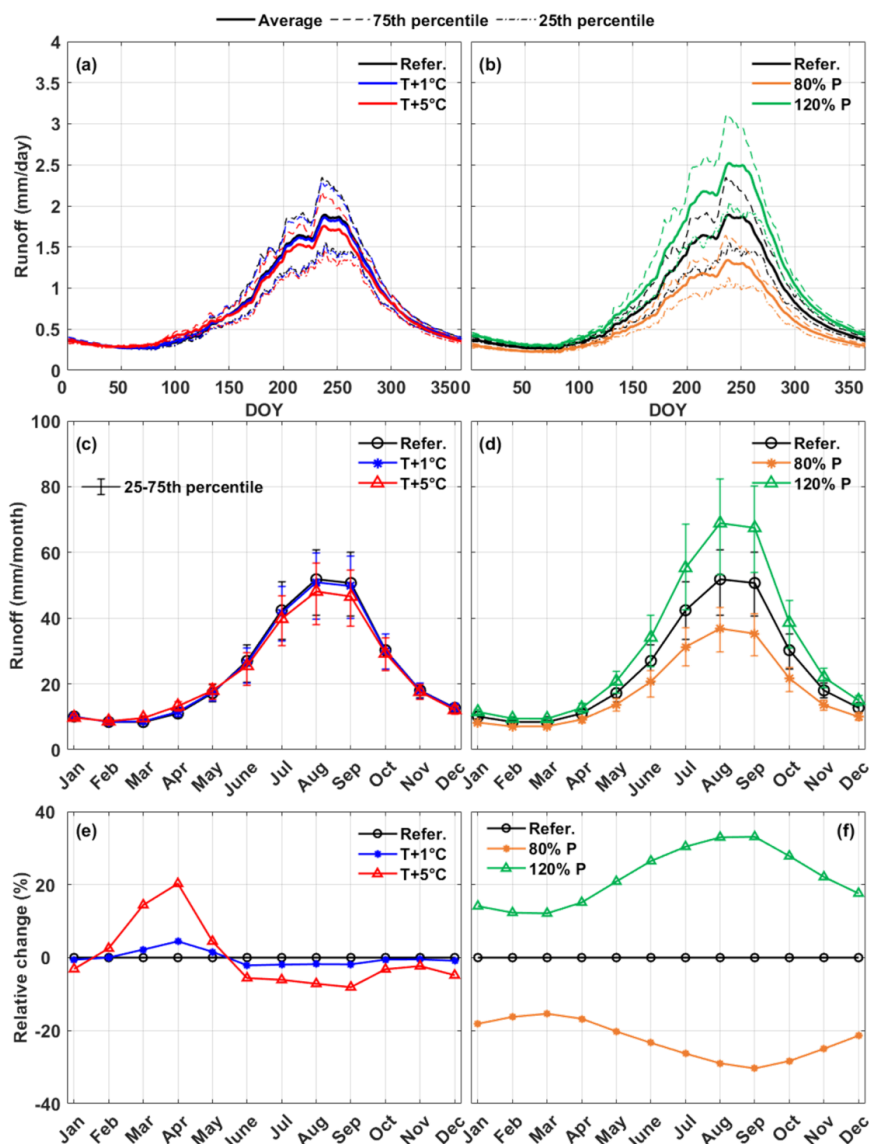
328 The hydrological sensitivities to perturbed precipitation were opposite to that of
 329 temperature. The annual runoff increased at the rate of 38.4 mm/10% with the increasing
 330 precipitation (Figure 4e). The relative change in runoff was larger than precipitation (Figure
 331 4h), indicating an increasing runoff coefficient with increasing precipitation. This also indicated
 332 a small relative change in evaporation in response to precipitation perturbation, again
 333 suggesting that the evaporation in this region was not limited by the water condition in the
 334 reference scenario. With the increasing precipitation, the snow cover area increased at
 335 0.7%/10%, and the glacier mass balance got more positive at 0.014m/10% because of the larger
 336 amount of snowfall and snow/ice accumulation (Figure 4f and 4g). Among the three variables,
 337 the runoff had the highest sensitivity to perturbed precipitation, with a relative change rate of
 338 13%/10% (Figure 4h), while the changes of snow cover area and glacier mass balance were
 339 within the range of $\pm 10\%$ when precipitation changed by 20%.

340 3.3 Sensitivities of runoff variation to perturbed temperature and precipitation

341 The sensitivities of inter- and intra-annual runoff variation to perturbed temperature and
 342 precipitation are shown in Figure 5. The average daily and monthly runoff were calculated
 343 based on the simulated hydrographs during the entire simulation period, and the inter-annual



344 runoff variation was represented by the 75th and 25th percentiles. The change of inter-annual
345 runoff variation was consistent with that of total runoff. The inter-annual runoff variations were
346 also lower in the scenarios with less runoff (increasing temperature or decreasing precipitation),
347 showing the narrower range between the 75th and 25th percentiles, and vice versa (Figure 5a-d).
348 Despite the decreasing runoff caused by increasing temperature, the average runoff for 5°C of
349 warming was still much higher than the 75th percentile of the reference scenario (Figure 5a and
350 5c), suggesting that the runoff change tendency caused by the increasing temperature was
351 relatively small compared to the inherent runoff variability. On the contrary, when precipitation
352 increased by 20%, the average annual runoff was higher than the runoff in wet years of reference
353 scenario (Figure 5b and 5d), indicating that the trend of precipitation change had a larger
354 influence on the runoff than the inter-annual variation of precipitation.



355
 356 **Figure 5.** Sensitivities of intra- and inter-annual streamflow variability to the perturbed
 357 temperature and precipitation. (a) and (b) daily runoff, (c) and (d) monthly runoff, (e) and (f)
 358 relative change of monthly runoff. The dash lines in (a)(b) and error bars in (c)(d) represent the
 359 75th and 25th percentiles during 2001-2015.

360 The sensitivities of monthly runoff were different among months. Although increasing
 361 temperature led to a decrease in the total runoff, it caused an increasing spring runoff. The



362 monthly runoff in April increased most significantly, which increased 20% for 5°C of warming
363 (Figure 5e). The monthly runoff in all twelve months changed accordingly to perturbed
364 precipitation, but the change during wet seasons (August to October) was the most significant
365 (Figure 5f). As a result, increasing temperature caused a more even distribution of monthly
366 runoff, while increasing precipitation had the opposite effect. The concentration ratio (CR) and
367 concentration period (CP) (Jiang et al., 2022) were calculated to characterize the runoff
368 seasonality (Table 4). The CR decreased from 0.432 to 0.402 for the warming of 5°C, indicating
369 a more even seasonal runoff distribution caused by increasing temperature. The CP decreased
370 by around two days, indicating that climate warming would result in advance of maximum
371 runoff. On the contrary, the CR changed from 0.398 to 0.465 when precipitation increased from
372 80% to 120% of the reference, indicating that increasing precipitation made the distribution of
373 runoff more concentrated. The CP advanced by 2.2 days in response to a 20% decreasing
374 precipitation, but only recessed by 0.3 days in response to an increasing precipitation with the
375 same magnitude.

376 **Table 4.** The concentration ratio (CR) and concentration period (CP) of runoff in different
377 scenarios with perturbed temperature and precipitation

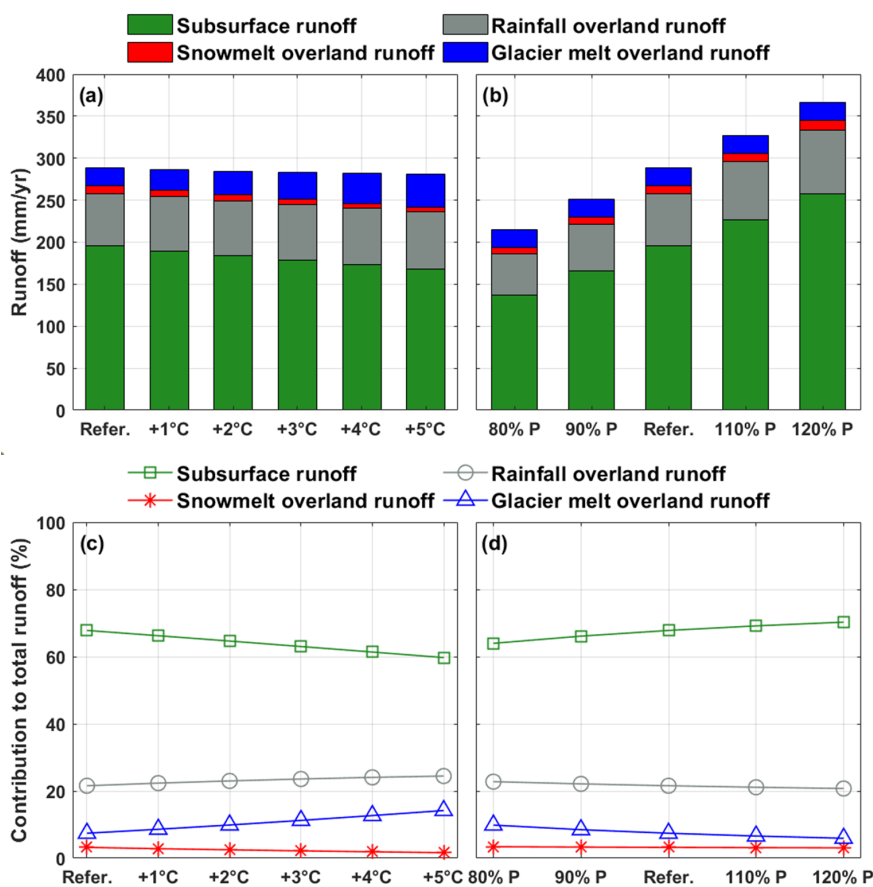
		CR	CP (days)
Reference scenario		0.432	244.4
T scenario	+1°C	0.425	244.1
	+2°C	0.419	243.8
	+3°C	0.413	243.3
	+4°C	0.408	242.8
	+5°C	0.402	242.3
P scenario	80%	0.398	242.2
	90%	0.415	243.6
	110%	0.449	244.7
	120%	0.465	244.7

378 3.4 Sensitivities of runoff components to perturbed temperature and precipitation

379 The contributions of runoff components in the YTR basin under scenarios with different
380 temperature and precipitation are shown in Figure 6. In the reference scenario, the subsurface
381 runoff was the dominant component, contributing about 70% to the total runoff. Among the
382 three surface runoff components, rainfall was the dominant water source contributing 20% to
383 the total runoff. Glacier melt overland runoff had considerable contribution to the runoff which



384 contributed about 10% to the total runoff, while the contribution of snowmelt overland runoff
 385 was smaller than 5%. The annual subsurface runoff was 195.8mm/yr (39.2 km³/yr), close to the
 386 amount (30 km³/s) estimated by Yao et al. (2021) with the groundwater model MODFLOW. It
 387 should be noted that in our model all the glacier meltwater was assumed to generate surface
 388 runoff directly because of the impermeable glacier surface, while the snowmelt was assumed
 389 to be partitioned into two components (infiltration and surface runoff) (Nan et al., 2021b, 2023;
 390 Schaefli et al., 2005).



391
 392 **Figure 6.** Sensitivities of the runoff components to perturbed temperature and precipitation.
 393 (a) and (b) amounts of runoff components, (c) and (d) contributions of runoff components to
 394 the total runoff.

395 With the increasing temperature, the amount and proportion of subsurface runoff decreased
 396 at -5.6mm/°C and -1.6%/°C, because climate warming increased evaporation and consequently

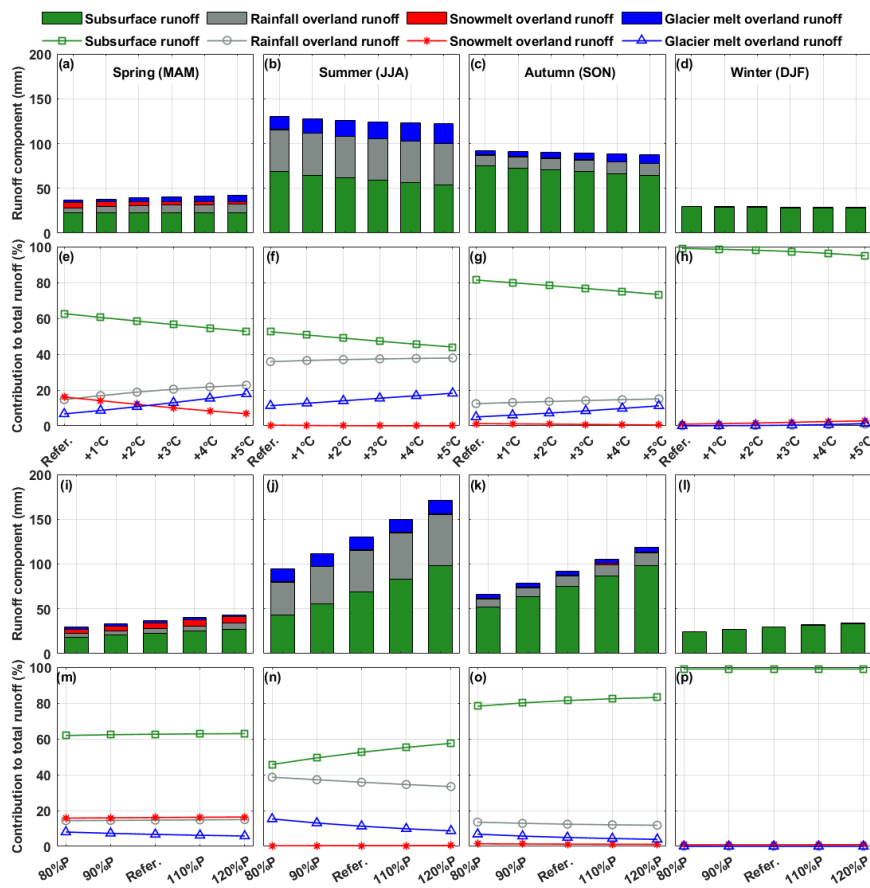


397 reduced the subsurface water storage and outflow. The rainfall and snowmelt overland runoff
398 increased at $1.3\text{mm}/^{\circ}\text{C}$ ($0.6\%/^{\circ}\text{C}$) and decreased at $-0.9\text{mm}/^{\circ}\text{C}$ ($-0.3\%/^{\circ}\text{C}$), respectively,
399 because more rainfall was partitioned from total precipitation due to higher temperature. The
400 glacier melt overland runoff increased significantly at $3.7\text{mm}/^{\circ}\text{C}$ ($1.4\%/^{\circ}\text{C}$) with the increasing
401 temperature, and the contribution to total runoff could be around 15% for 5°C of warming. The
402 amount of all four runoff components increased with the increasing precipitation (Figure 6b),
403 with rates of $30.1\text{mm}/10\%$, $6.8\text{mm}/10\%$, $1.0\text{mm}/10\%$ and $0.1\text{mm}/10\%$ for subsurface, rainfall
404 overland, snowmelt overland and glacier melt overland runoff, respectively. However, only the
405 proportion of subsurface runoff increased at $1.6\%/10\%$ with the increasing precipitation, while
406 the proportions of three other components all decreased, with rates of $-0.5\%/10\%$, $-0.1\%/10\%$
407 and $-1.0\%/10\%$ for rainfall overland, snowmelt overland and glacier melt overland runoff,
408 respectively (Figure 6d), because there was a much higher increase in the total runoff. Overall,
409 the contributions of runoff components were more sensitive to temperature perturbation than
410 precipitation perturbation.

411 Figure 7 shows the runoff components in different seasons and their sensitivities to
412 perturbed climate. The subsurface runoff was the dominant component in all four seasons in
413 the reference scenario, with contribution ranging from 53% in summer to 99% in winter. The
414 contribution of snowmelt overland runoff was extremely low in the seasons except for spring
415 because of the small SCA in summer and autumn and the low temperature in winter. The
416 contribution of snowmelt overland runoff in spring was close to that of rainfall overland runoff
417 (Figure 7e-h). The contribution of glacier melt overland runoff was around half that of rainfall
418 overland runoff in all four seasons. With climate warming, the contribution of subsurface runoff
419 decreased in all four seasons, while the contributions of rainfall and glacier melt overland runoff
420 increased. The significantly increasing glacier melt and rainfall led to an increase in the total
421 runoff in spring (Figure 7a). The contribution of snowmelt overland runoff decreased in three
422 seasons except for winter, during which its contribution slightly increased, and got around 3%
423 for 5°C of warming (Figure 7h). With increasing precipitation, the amounts of four components
424 increased in all seasons (Figure 7i-l), but the contributions of components remained nearly
425 unchanged in spring, autumn and winter (Figure 7m, o-p). The contributions of runoff
426 components were sensitive to perturbed precipitation only in summer, during which subsurface



427 runoff contributed more to the runoff with increasing precipitation, while the contributions of
 428 rainfall and glacier melt overland runoff decreased significantly (Figure 7n).



429
 430 **Figure 7.** Sensitivities of the seasonal runoff components to perturbed temperature and
 431 precipitation. (a)-(d) sensitivities of amounts of runoff components to perturbed temperature,
 432 (e)-(h) sensitivities of contributions of runoff components to perturbed temperature, (i)-(l)
 433 sensitivities of amounts of runoff components to perturbed precipitation, (m)-(p) sensitivities
 434 of contributions of runoff components to perturbed precipitation.

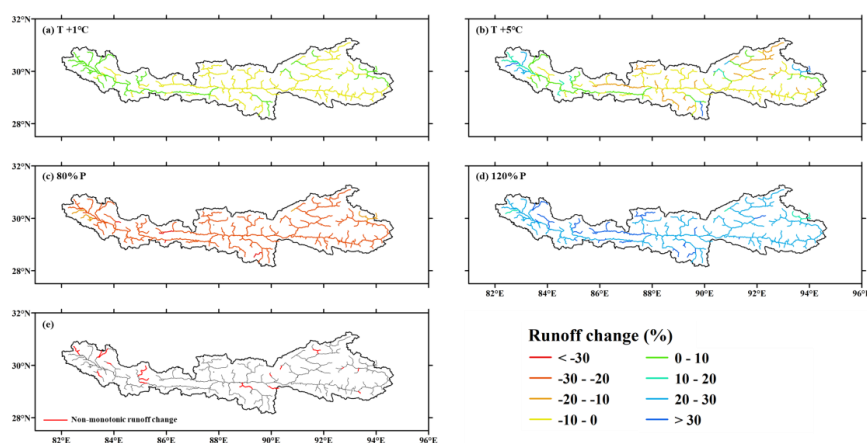
435 3.5 Spatial pattern of local hydrological sensitivities

436 Considering that the YTR basin is a large basin with drainage area of $2 \times 10^5 \text{ km}^2$, the spatial
 437 pattern of the local hydrological sensitivity was further analyzed with the assistance of the
 438 spatially distributed model structure. The runoff change at REW scale in four typical scenarios



439 (i.e., 1°C of warming, 5°C of warming, precipitation changing to 80% and 120%) are shown in
440 Figure 8. All REWs have the same runoff trend with the precipitation perturbation (Figure 8c
441 and 8d). The runoff increasing ranged from 12.2% to 40.4% when precipitation increased by
442 20%. In most REWs, the runoff changed at larger rates than precipitation, with few exceptions
443 located in the tributaries of Nyang River, Lhasa River and the source region of mainstream,
444 showing shallow red/blue colors in Figure 8c and 8d. On the contrary, the REW scale runoff
445 changes in response to increasing temperature had strong spatial variability (Figure 8a and 8b).
446 Although the runoff at the basin outlet decreased with climate warming, the REW scale runoff
447 increased in about half of REWs. For 5°C of warming, the REW scale runoff changes ranged
448 from -18.6% to 54.3%. Most REWs with increasing runoff were located upstream of the
449 mainstream, the Nianchu River, the Nyang River, and the tributary of Lhasa River (Figure 8b).

450 The runoff in some REWs changed non-monotonically with increasing temperature, i.e.,
451 the runoff change trend was reversed in different temperature intervals. Most of such non-
452 monotonic REWs were located in the upstream region of the mainstream, with some others
453 located in the major tributaries Nyang River, Lhasa River and Nianchu River (Figure 8e). In
454 about 75% of non-monotonic REWs, the runoff first decreased for 1°C of warming, and then
455 changed to an increasing trend at higher warming levels, and the reserved trends occurred in
456 the other 25% of REWs. The threshold temperature of trend turning differed among non-
457 monotonic REWs, which was 3°C in about half of the REWs. The runoff change rates in
458 response to increasing temperature were generally low in non-monotonic REWs, most within
459 the range of $\pm 1\%/^{\circ}\text{C}$.



460

461 **Figure 8.** The change of REW scale runoff in response to perturbed temperature and
462 precipitation. (a) and (b) runoff change in response to temperature perturbation, (c) and (d)
463 runoff change in response to precipitation perturbation, (e) the locations of REWs showing non-
464 monotonic runoff change in response to increasing temperature.

465 4. Discussions

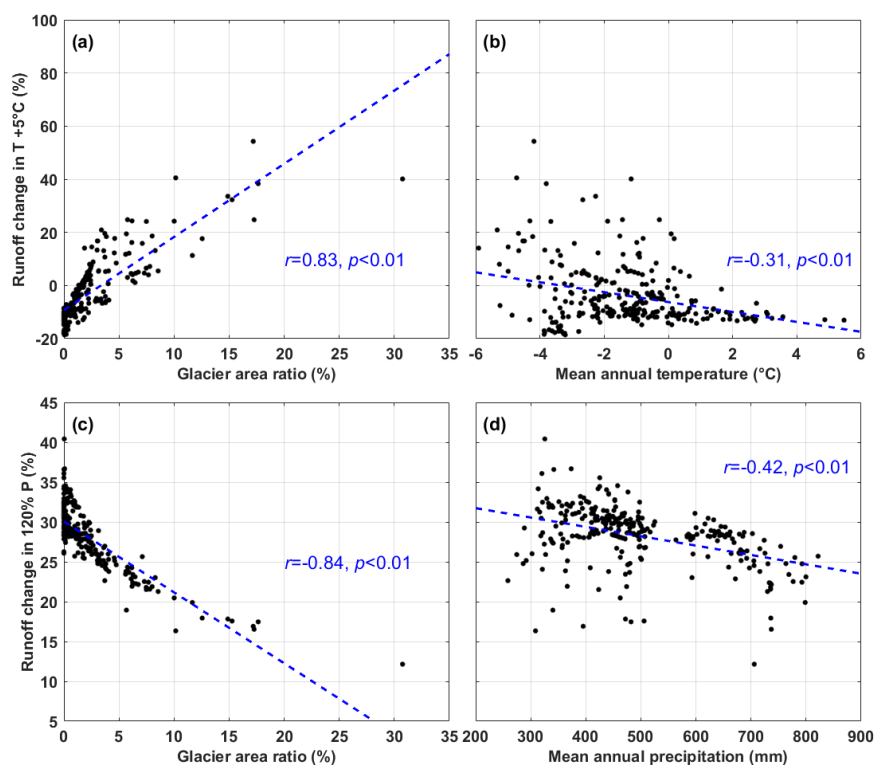
466 4.1 The influence factors of local hydrological sensitivities: the role of glaciers

467 Our results show the strong spatial variability of the REW scale hydrological sensitivities
468 to perturbed climate. Consequently, the influence factors of the local sensitivities are analyzed
469 in this section. The basic characteristics, including mean annual temperature (MAT), mean
470 annual precipitation (MAP), average elevation (ELE), drainage area (DRA), and glacier area
471 ratio (GAR) were calculated for each REW as the potential factors. It should be noted that,
472 considering the runoff concentration processes between the upstream and downstream REWs,
473 the above characteristics were not calculated solely within each REW, but for the total drainage
474 area controlled by each REW. The correlations between the runoff change for
475 temperature/precipitation increasing by 5°C/20% and the potential influence factors were
476 analyzed, and the relations with the two factors with the highest coefficients are shown in Figure
477 9.

478 The GAR was the most correlated factor for the hydrological sensitivities to the
479 perturbation of both temperature and precipitation, with coefficients higher than 0.8 (Figure 9a
480 and 9c). The runoff change for 5°C of warming increased with the increasing GAR (Figure 9a),



481 because of the balance between the decreasing runoff caused by evaporation and the increasing
482 runoff contributed by glacier melt. In REWs where the GAR was higher than a threshold, the
483 increasing glacier melt could offset the increasing evaporation, and the runoff increased with
484 climate warming. The threshold GAR was different among REWs, ranging from 1-5%. For the
485 REWs with GAR larger than 10%, the runoff increase for 5°C of warming could be higher than
486 20%. The hydrological sensitivity to increasing temperature also had a weak but significant
487 negative correlation ($p < 0.01$) with the MAT of the REW (Figure 9b), which could be partly
488 attributed to the interrelation between GAR and MAT, i.e., the GAR tended to be higher in
489 warmer regions, and the runoff consequently decreased in response to increasing temperature.
490 A lower bound of runoff change could be observed in Figure 9b for the REWs with relatively
491 high MAT, again indicating the different limitation factors of evaporation, i.e., in relatively
492 warm regions, the evaporation was limited by the water condition, so increasing temperature
493 did not cause more evaporation (Wang et al., 2022).



494

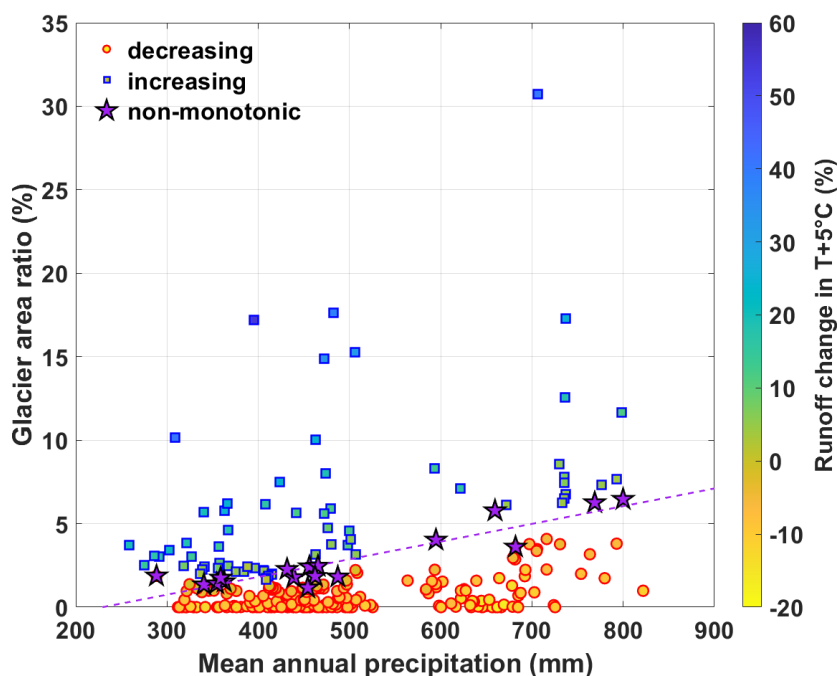
495 **Figure 9.** The correlations between the hydrological sensitivities to climate perturbation and



496 the dominant influence factors.

497 On the contrary, the runoff change in response to increasing precipitation had a negative
498 correlation with the GAR (Figure 9c), mainly due to the spatial variability of the runoff
499 components. In REWs with larger GAR, the contribution of precipitation-induced runoff was
500 relatively low due to the large contribution of glacier melt runoff, thus the influence of
501 increasing precipitation on runoff change was also small. Meanwhile, the runoff change in
502 response to increasing temperature also negatively correlated with the MAP (Figure 9d). The
503 contribution of subsurface runoff component was higher in wetter conditions (Figure 6d),
504 resulting in more evaporation and a lower runoff coefficient, which caused a relatively small
505 increase in runoff, similar with the finding by He et al. (2021b).

506 Our results indicate that the runoff in some REWs changed non-monotonically in response
507 to the increasing temperature. The characteristics of these non-monotonic REWs were further
508 analyzed. Interestingly, the GAR of non-monotonic REWs has a good linear relationship with
509 their MAP (Figure 10). The regression equation of the linear relation was
510 $GAR(\%)=0.011*MAP(mm)-2.43$ ($r=0.92$). Moreover, this regression line was the dividing line
511 between the REWs where runoff increased with increasing temperature and those with opposite
512 runoff trends in the GAR-MAP plot (Figure 10). The REWs located in the upper part of the plot
513 had larger runoff increasing rates. This indicated that the local hydrological sensitivity to
514 increasing temperature was determined by the relationship between GAR and MAP. In wetter
515 REWs with larger MAP, more glaciers were needed to offset the decreasing runoff due to the
516 increasing temperature and evaporation. These findings suggested the important role of glaciers
517 in determining the runoff change in response to climate change.



518

519 **Figure 10.** The interrelation among the REW scale glacier area ratio, mean annual
520 precipitation and the runoff change for 5°C of warming.

521 4.2 Implications of the sensitivity analysis

522 The sensitivity analysis indicated the important role of glaciers in providing meltwater to
523 offset the runoff decreasing caused by climate warming. Our study showed that glacier
524 meltwater had a limited contribution to the total runoff in the YTR basin, similar with some
525 recent studies (Wang et al., 2021; Cui et al., 2023), resulting in a decreasing runoff trend with
526 increasing temperature. However, the spatial pattern analysis indicated that the role of glacier
527 melt runoff could be rather significant in the regions with large area covered by glaciers. For
528 example, the runoff increased significantly in the Yangbajing tributary of the Lhasa River in
529 response to increasing temperature (Figure 8), consistent with previous research estimating a
530 high contribution of glacier melt to runoff in this region (Lin et al., 2020; Wang et al., 2023). It
531 is therefore necessary to address the spatial scale issue when discussing the role of glacier
532 meltwater on water resources.

533 Several studies have stressed the important role of glaciers on the TP as the largest global



534 store of frozen water which supplied freshwater resources to downstream regions (Yao et al.,
535 2022). This study quantitatively estimated the role of glacier meltwater in offsetting the
536 decreasing runoff with increasing temperature and evaporation. Our results indicated that the
537 influences of glacier on hydrological processes were highly dependent on the spatial scale and
538 the local meteorological characteristics. Specifically, the role of glacier meltwater would
539 undoubtedly be more significant in regions with larger glacier cover areas (Luo et al., 2018;
540 Zhao et al., 2019; Khanal et al., 2021). Meanwhile, the role of glaciers was smaller in wetter
541 regions with higher precipitation because of the relatively low contribution of glacier meltwater
542 in total runoff. Consequently, the regions with larger precipitation amounts but little glacier
543 coverage would face a greater risk of water resources shortage in a warming future. Our results
544 also suggested a larger influence of precipitation change on runoff than that of temperature
545 change (Figure 4), thus an accurate projection of precipitation is crucial for the assessment of
546 water resources under climate change. Recent studies showed a decreasing precipitation trend
547 after 2000 in the YTR basin (Li et al., 2016; Luan and Zhai, 2022), likely posing threats of
548 water scarcity to the riparian regions and again highlighting the important role of glacier in
549 maintaining water resources.

550 Our results showed that the runoff responded to increasing temperature non-monotonically
551 in some regions. Recent studies also projected the non-monotonic runoff change on the TP at
552 increasing warming levels (Cui et al., 2023), i.e., the annual mean runoff for major rivers on
553 the TP will decrease by 0.1-3.2% at the warming level of 1.5°C, and increase by 1.5-12% at
554 3.0°C in the future. Although seemingly similar, the two studies revealed two different
555 phenomena. In particular, the non-monotonic runoff change projected by Cui et al. (2023) was
556 driven by the output put of climatic projection data CMIP6 (Eyring et al., 2016), and the runoff
557 change was dominated by the tendencies and periodicities of climate factors, especially
558 precipitation (Wu et al., 2022). Our study analyzed the runoff change in response to climate
559 warming with fixed precipitation input, and the trend was the result of the comprehensive
560 response of multiple water balance components to climate change. The local non-monotonic
561 hydrological sensitivity was essentially a borderline condition of increasing and decreasing
562 trend, which reflected the balance of increasing meltwater and evaporation in response to
563 climate warming.



564

565 **4.3 Limitations**

566 This study explored the sensitivities of hydrological processes to climate change by
567 designing temperature and precipitation perturbation scenarios, rather than projecting future
568 runoff using the forcing data from general circulation models (GCMs). The assumed climate
569 perturbation method is widely used in runoff projection studies (He et al., 2021b; Su et al., 2023;
570 Rasouli et al., 2014; Rasouli et al., 2015), with the advantage of avoiding the computation cost
571 of correcting biases and downscaling GCMs to regional scale (Piani et al., 2010; Xu et al.,
572 2019). However, the assumed climate perturbation did not reflect the gradual process of climate
573 change. Specifically, the temperature should go through relatively low warming levels before
574 arriving at the assumed highest level, but the climate perturbation method actually assumed an
575 abrupt climate change. We can expect that the role of glaciers when temperature increases by
576 5°C in the future should be less than our results, because the glacier covered area at that time
577 will be less than the current condition (Yao et al., 2022). Meanwhile, the potential influences
578 of temperature and precipitation change on soil and vegetation conditions (Boulanger et al.,
579 2016) were not considered when designing the climate perturbation scenarios. Nonetheless, the
580 simple sensitivity analysis in this study helped better understand the separate effect of changing
581 temperature and precipitation on runoff, and informed the role of glaciers in controlling the
582 spatial pattern of runoff change.

583 Another limitation comes from the uncertainties of hydrological model. Although
584 validated by the measurement data of multiple objectives and several internal stations, the
585 model still had potential uncertainties. First, as the most important forcing data, the common
586 precipitation datasets in the YTR basin all had large uncertainties, due to the lack of validation
587 data in high elevation regions (Xu et al., 2017), leading to uncertainties in hydrological
588 simulation. Second, because of the complex hydrological processes and runoff components, the
589 parameter equifinality problem usually existed in the hydrological model in large mountainous
590 basins (Gupta et al., 2008; Nan et al., 2021a). He et al. (2019) indicated that the uncertainties
591 of runoff component contributions could be nearly 20% even when the simulations of
592 streamflow, snow, glacier and isotope were satisfied simultaneously. The misestimation of the



593 runoff regime would undoubtedly influence the sensitivity analysis. Lastly, the calibrated
594 parameters were assumed to be spatially uniform within the whole basin to avoid introducing
595 too many parameters. Although this is similar to several large-scale modeling studies (e.g., Cui
596 et al., 2023; Lutz et al., 2014), the uniform parameter might be inadequate to represent the
597 spatial variability of hydrological processes, which may influence some conclusions of the
598 sensitivity analysis. For example, considering the potential spatial variability of glacier melting
599 rate, the characteristics of non-monotonic REWs in Figure 10 may not form a straight line.

600 5. Conclusions

601 This study adopted the tracer-aided hydrological model THREW-T in a typical large
602 mountainous basin Yarlung Tsangpo River (YTR) on the Tibetan Plateau (TP). The model was
603 validated against multiple objectives (streamflow, snow, glacier and isotope) and the
604 streamflow at internal stations. The sensitivities of hydrological processes to perturbed
605 temperature and precipitation were analyzed. The spatial pattern of local hydrological
606 sensitivities and the influence factors were explored. Our main findings are as follows:

607 (1) The THREW-T model performed well on simulating the streamflow, snow cover area
608 (SCA), glacier mass balance (GMB), and stream water isotope, ensuring good representation
609 of the key cryospheric processes and a reasonable estimation of the contributions of runoff
610 components. The model performed acceptably on simulating the streamflow at eight internal
611 stations located in the mainstream and two major tributaries, which indicated that the spatial
612 pattern of hydrological processes was reflected by the model, and provided confidence in the
613 sensitivity analysis.

614 (2) Most hydrological characteristics responded to increasing temperature and
615 precipitation oppositely. Increasing temperature led to decreasing annual runoff, SCA and GMB,
616 and changed the runoff variation showing a smaller inter-annual variation, a more even
617 distributed intra-annual distribution, and an earlier maximum runoff. It also influenced the
618 runoff regime by increasing the contributions of rainfall and glacier melt overland runoff, but
619 decreasing the subsurface runoff and snowmelt overland runoff. Increasing precipitation had
620 the opposite effects to increasing temperature.

621 (3) The distribution of local hydrological sensitivities had a strong spatial variability. The



622 local runoff change in response to increasing temperature varied significantly, with changing
623 rate of -18.6% to 54.3% for 5°C of warming. The glacier area ratio (GAR) was the dominant
624 factor of the spatial pattern of hydrological sensitivities to both perturbed temperature and
625 precipitation. Some regions had a non-monotonic runoff trend in response to increasing
626 temperature, the GAR and mean annual precipitation (MAP) of which showed linear relation,
627 and formed the boundary of regions with different trends with increasing temperature in the
628 GAR-MAP plot.

629

630 **Code and data availability**

631 Code and data availability. The isotope data and the code of THREW-T model used in this study
632 are available from the corresponding author (tianfq@tsinghua.edu.cn). Other data sets are
633 publicly available as follows: DEM (<http://www.gscloud.cn/sources/details/310?pid=302>, last
634 access: 1 January 2019, Geospatial Data Cloud Site, 2019), CMFD
635 (<https://doi.org/10.11888/AtmosphericPhysics.tpe.249369.file>, Yang and He, 2019), glacier
636 inventory data (<https://doi.org/10.3972/glacier.001.2013.db>, Liu, 2012), glacier elevation
637 change data (<https://doi.org/10.6096/13>, Huggonet et al., 2021), NDVI
638 (<https://doi.org/10.5067/MODIS/MOD13A3.006>, Didan, 2015), LAI
639 (<https://doi.org/10.5067/MODIS/MOD15A2H.006>, Myneni et al., 2015), HWSD
640 (<https://data.tpc.ac.cn/zh-hans/data/3519536a-d1e7-4ba1-8481-6a0b56637baf/?q=HWSD>,
641 last access: 1 January 2019, He, 2019). These datasets not publicly available are referred to in
642 the main text (Chen et al., 2018; Liu et al., 2007).

643

644 **Author contribution**

645 YN conceived the idea and collected data; YN and FT conducted analysis and wrote the paper.

646

647 **Financial support**

648 This study has been supported by the National Natural Science Foundation of China (grant no.
649 92047301) and the Shuimu Tsinghua Scholar Program.

650



651 **Competing interests**

652 At least one of the (co-)authors is a member of the editorial board of Hydrology and Earth
653 System Sciences.

654

655 **References**

656 Aygun, O., Kinnard, C., Campeau, S., and Krogh, S. A.: Shifting Hydrological Processes in a
657 Canadian Agroforested Catchment due to a Warmer and Wetter Climate, *Water*, 12,
658 10.3390/w12030739, 2020.

659 Bai, X. L., Zhao, W. Z., Liu, H., Zhang, Y. Y., Yang, Q. Y., Liu, J. T., and Chang, X. L.: Effects
660 of precipitation changes and land-use alteration on streamflow: A comparative analysis
661 from two adjacent catchments in the Qilian Mountains, arid northwestern China, *Frontiers
662 in Environmental Science*, 11, 10.3389/fenvs.2023.1097049, 2023.

663 Birkel, C. and Soulsby, C.: Advancing tracer-aided rainfall-runoff modelling: a review of
664 progress, problems and unrealised potential, *Hydrological Processes*, 29, 5227-5240,
665 10.1002/hyp.10594, 2015.

666 Bloschl, G. and Montanari, A.: Climate change impacts-throwing the dice?, *Hydrological
667 Processes*, 24, 374-381, 10.1002/hyp.7574, 2010.

668 Boulanger, Y., Taylor, A. R., Price, D. T., Cyr, D., McGarrigle, E., Rammer, W., Sainte-Marie,
669 G., Beaudoin, A., Guindon, L., and Mansuy, N.: Climate change impacts on forest
670 landscapes along the Canadian southern boreal forest transition zone, *Landscape Ecology*,
671 32, 1415-1431, 10.1007/s10980-016-0421-7, 2017.

672 Cao, L. G. and Pan, S. M.: Changes in precipitation extremes over the "Three-River
673 Headwaters" region, hinterland of the Tibetan Plateau, during 1960-2012, *Quaternary
674 International*, 321, 105-115, 10.1016/j.quaint.2013.12.041, 2014.

675 Chen, X., Long, D., Liang, S., He, L., Zeng, C., Hao, X., and Hong, Y.: Developing a composite
676 daily snow cover extent record over the Tibetan Plateau from 1981 to 2016 using
677 multisource data, *Remote Sensing of Environment*, 215, 284-299,
678 10.1016/j.rse.2018.06.021, 2018.

679 Cui, T., Li, Y., Yang, L., Nan, Y., Li, K., Tudaji, M., Hu, H., Long, D., Shahid, M., Mubeen, A.,



- 680 He, Z., Yong, B., Lu, H., Li, C., Ni, G., Hu, C., and Tian, F.: Non-monotonic changes in
681 Asian Water Towers' streamflow at increasing warming levels, *Nature communications*,
682 14, 1176-1176, 10.1038/s41467-023-36804-6, 2023.
- 683 Didan, K.: MOD13A3 MODIS/Terra vegetation Indices Monthly L3 Global 1 km SIN Grid
684 V006, NASA EOSDIS Land Processes DAAC [dataset],
685 <https://doi.org/10.5067/MODIS/MOD13A3.006>, 2015.
- 686 Eyring, V., Bony, S., Meehl, G. A., Senior, C. A., Stevens, B., Stouffer, R. J., and Taylor, K. E.:
687 Overview of the Coupled Model Intercomparison Project Phase 6 (CMIP6) experimental
688 design and organization, *Geoscientific Model Development*, 9, 1937-1958, 10.5194/gmd-
689 9-1937-2016, 2016.
- 690 Fassnacht, S. R., Sexstone, G. A., Kashipazha, A. H., Ignacio Lopez-Moreno, J., Jasinski, M.
691 F., Kampf, S. K., and Von Thaden, B. C.: Deriving snow-cover depletion curves for
692 different spatial scales from remote sensing and snow telemetry data, *Hydrological
693 Processes*, 30, 1708-1717, 10.1002/hyp.10730, 2016.
- 694 Gao, J., Yao, T. D., Masson-Delmotte, V., Steen-Larsen, H. C., and Wang, W. C.: Collapsing
695 glaciers threaten Asia's water supplies, *Nature*, 565, 19-21, 10.1038/d41586-018-07838-4,
696 2019.
- 697 Gupta, H. V., Wagener, T., and Liu, Y.: Reconciling theory with observations: elements of a
698 diagnostic approach to model evaluation, *Hydrological Processes*, 22, 3802-3813,
699 10.1002/hyp.6989, 2008.
- 700 He, Y.: Pan-TPE soil map based on Harmonized World Soil Database (V1.2), National Tibetan
701 Plateau Data Center [dataset], 2019.
- 702 He, Z. H. and Pomeroy, J. W.: Assessing hydrological sensitivity to future climate change over
703 the Canadian southern boreal forest, *Journal of Hydrology*, 624,
704 10.1016/j.jhydrol.2023.129897, 2023.
- 705 He, Z., Duethmann, D., and Tian, F.: A meta-analysis based review of quantifying the
706 contributions of runoff components to streamflow in glacierized basins, *Journal of
707 Hydrology*, 603, 10.1016/j.jhydrol.2021.126890, 2021.
- 708 He, Z. H., Pomeroy, J. W., Fang, X., and Peterson, A.: Sensitivity analysis of hydrological
709 processes to perturbed climate in a southern boreal forest basin, *Journal of Hydrology*, 601,



- 710 10.1016/j.jhydrol.2021.126706, 2021.
- 711 He, Z., Unger-Shayesteh, K., Vorogushyn, S., Weise, S. M., Kalashnikova, O., Gafurov, A.,
712 Duethmann, D., Barandun, M., and Merz, B.: Constraining hydrological model parameters
713 using water isotopic compositions in a glacierized basin, Central Asia, *Journal of*
714 *Hydrology*, 571, 332-348, 10.1016/j.jhydrol.2019.01.048, 2019.
- 715 Hindshaw, R. S., Tipper, E. T., Reynolds, B. C., Lemarchand, E., Wiederhold, J. G., Magnusson,
716 J., Bernasconi, S. M., Kretzschmar, R., and Bourdon, B.: Hydrological control of stream
717 water chemistry in a glacial catchment (Damma Glacier, Switzerland), *Chemical Geology*,
718 285, 215-230, 10.1016/j.chemgeo.2011.04.012, 2011.
- 719 Hugonnet, R., McNabb, R., Berthier, E., Menounos, B., Nuth, C., Girod, L., Farinotti, D., Huss,
720 M., Dussailant, I., Brun, F., and Kaab, A.: Accelerated global glacier mass loss in the early
721 twenty-first century, *Nature*, 592, 726+, 10.1038/s41586-021-03436-z, 2021.
- 722 Immerzeel, W. W., van Beek, L. P. H., and Bierkens, M. F. P.: Climate Change Will Affect the
723 Asian Water Towers, *Science*, 328, 1382-1385, 10.1126/science.1183188, 2010.
- 724 Jiang, Y., Xu, Z., and Xiong, L.: Runoff variation and response to precipitation on multi-spatial
725 and temporal scales in the southern Tibetan Plateau, *Journal of Hydrology-Regional*
726 *Studies*, 42, 10.1016/j.ejrh.2022.101157, 2022.
- 727 Khanal, S., Lutz, A. F., Kraaijenbrink, P. D. A., van den Hurk, B., Yao, T., and Immerzeel, W.
728 W.: Variable 21st Century Climate Change Response for Rivers in High Mountain Asia at
729 Seasonal to Decadal Time Scales, *Water Resources Research*, 57, 10.1029/2020wr029266,
730 2021.
- 731 Li, X., Yao, Z., Xiao, J., and Wang, H.: Analysis of the spatial-temporal variation characteristics
732 of precipitation over the Tibetan Plateau from 1961 through 2010, *Journal of Glaciology*
733 *and Geocryology*, 38, 1233-1240, 2016.
- 734 Li, C., Sinha, E., Horton, D. E., Diffenbaugh, N. S., and Michalak, A. M.: Joint bias correction
735 of temperature and precipitation in climate model simulations, *Journal of Geophysical*
736 *Research-Atmospheres*, 119, 13153-13162, 10.1002/2014jd022514, 2014.
- 737 Li, Z. X., Feng, Q., Li, Z. J., Yuan, R. F., Gui, J., and Lv, Y. M.: Climate background, fact and
738 hydrological effect of multiphase water transformation in cold regions of the Western
739 China: A review, *Earth-Science Reviews*, 190, 33-57, 10.1016/j.earscirev.2018.12.004,



- 740 2019.
- 741 Li, Z. J., Li, Z. X., Song, L. L., Gui, J., Xue, J., Zhang, B. J., and Gao, W. D.: Hydrological and
742 runoff formation processes based on isotope tracing during ablation period in the source
743 regions of Yangtze River, *Hydrology and Earth System Sciences*, 24, 4169-4187,
744 10.5194/hess-24-4169-2020, 2020.
- 745 Li, K., Tian, F., Khan, M. Y. A., Xu, R., He, Z., Yang, L., Lu, H., and Ma, Y.: A high-accuracy
746 rainfall dataset by merging multiple satellites and dense gauges over the southern Tibetan
747 Plateau for 2014-2019 warm seasons, *Earth System Science Data*, 13, 5455-5467,
748 10.5194/essd-13-5455-2021, 2021.
- 749 Lin, L., Gao, M., Liu, J., Wang, J., Wang, S., Chen, X., and Liu, H.: Understanding the effects
750 of climate warming on streamflow and active groundwater storage in an alpine catchment:
751 the upper Lhasa River, *Hydrology and Earth System Sciences*, 24, 1145-1157,
752 10.5194/hess-24-1145-2020, 2020.
- 753 Liu, S.: The second glacier inventory dataset of China (version 1.0) (2006–2011), National
754 Tibetan Plateau Data Center [dataset], 10.3972/glacier.001.2013.db, 2012.
- 755 Liu, Z. F., Tian, L. D., Yao, T. D., Gong, T. L., Yin, C. L., and Yu, W. S.: Temporal and spatial
756 variations of delta O-18 in precipitation of the Yarlung Zangbo River Basin, *Journal of*
757 *Geographical Sciences*, 17, 317-326, 10.1007/s11442-007-0317-1, 2007.
- 758 Luan, L. and Zhai, P.: Changes in rainy season precipitation properties over the Qinghai-Tibet
759 Plateau based on multi-source datasets, *Progressus Inquisitiones de Mutatione Climatis*,
760 19, 173-190, 2023.
- 761 Luo, Y., Arnold, J., Liu, S., Wang, X., and Chen, X.: Inclusion of glacier processes for
762 distributed hydrological modeling at basin scale with application to a watershed in
763 Tianshan Mountains, northwest China, *Journal of Hydrology*, 477, 72-85,
764 10.1016/j.jhydrol.2012.11.005, 2013.
- 765 Luo, Y., Arnold, J., Liu, S. Y., Wang, X. Y., and Chen, X.: Inclusion of glacier processes for
766 distributed hydrological modeling at basin scale with application to a watershed in
767 Tianshan Mountains, northwest China, *Journal of Hydrology*, 477, 72-85,
768 10.1016/j.jhydrol.2012.11.005, 2013.
- 769 Luo, Y., Wang, X., Piao, S., Sun, L., Ciais, P., Zhang, Y., Ma, C., Gan, R., and He, C.:



- 770 Contrasting streamflow regimes induced by melting glaciers across the Tien Shan - Pamir
771 - North Karakoram, Scientific Reports, 8, 10.1038/s41598-018-34829-2, 2018.
- 772 Luo, Y., Wang, X. L., Piao, S. L., Sun, L., Ciais, P., Zhang, Y. Q., Ma, C. K., Gan, R., and He,
773 C. S.: Contrasting streamflow regimes induced by melting glaciers across the Tien Shan -
774 Pamir - North Karakoram, Scientific Reports, 8, 10.1038/s41598-018-34829-2, 2018.
- 775 Lutz, A. F., Immerzeel, W. W., Shrestha, A. B., and Bierkens, M. F. P.: Consistent increase in
776 High Asia's runoff due to increasing glacier melt and precipitation, Nature Climate Change,
777 4, 587-592, 10.1038/nclimate2237, 2014.
- 778 Myneni, R., Knyazikhin, Y., and Park, T.: MOD15A2H MODIS/Terra Leaf Area Index/FPAR
779 8-Day L4 Global 500 m SIN Grid V006, NASA EOSDIS Land Processes DAAC [dataset],
780 10.5067/MODIS/MOD15A2H.006, 2015.
- 781 Nan, Y., Tian, F., Li, Z., and Gui, J.: Longer simulation time step of the tracer-aided hydrological
782 model estimates lower contribution of slow runoff components, Journal of Hydrology,
783 <https://doi.org/10.1016/j.jhydrol.2023.129889>, 2023.
- 784 Nan, Y., He, Z., Tian, F., Wei, Z., and Tian, L.: Can we use precipitation isotope outputs of
785 isotopic general circulation models to improve hydrological modeling in large
786 mountainous catchments on the Tibetan Plateau?, Hydrology and Earth System Sciences,
787 25, 6151-6172, 10.5194/hess-25-6151-2021, 2021.
- 788 Nan, Y., He, Z., Tian, F., Wei, Z., and Tian, L.: Assessing the influence of water sampling
789 strategy on the performance of tracer-aided hydrological modeling in a mountainous basin
790 on the Tibetan Plateau, Hydrology and Earth System Sciences, 26, 4147-4167,
791 10.5194/hess-26-4147-2022, 2022.
- 792 Nan, Y., Tian, L., He, Z., Tian, F., and Shao, L.: The value of water isotope data on improving
793 process understanding in a glacierized catchment on the Tibetan Plateau, Hydrology and
794 Earth System Sciences, 25, 3653-3673, 10.5194/hess-25-3653-2021, 2021.
- 795 Olsson, T., Jakkila, J., Veijalainen, N., Backman, L., Kaurola, J., and Vehvilainen, B.: Impacts
796 of climate change on temperature, precipitation and hydrology in Finland - studies using
797 bias corrected Regional Climate Model data, Hydrology and Earth System Sciences, 19,
798 3217-3238, 10.5194/hess-19-3217-2015, 2015.
- 799 Piani, C., Weedon, G. P., Best, M., Gomes, S. M., Viterbo, P., Hagemann, S., and Haerter, J. O.:



- 800 Statistical bias correction of global simulated daily precipitation and temperature for the
801 application of hydrological models, *Journal of Hydrology*, 395, 199-215,
802 10.1016/j.jhydrol.2010.10.024, 2010.
- 803 Rasouli, K., Pomeroy, J. W., and Marks, D. G.: Snowpack sensitivity to perturbed climate in a
804 cool mid-latitude mountain catchment, *Hydrological Processes*, 29, 3925-3940,
805 10.1002/hyp.10587, 2015.
- 806 Rasouli, K., Pomeroy, J. W., Janowicz, J. R., Carey, S. K., and Williams, T. J.: Hydrological
807 sensitivity of a northern mountain basin to climate change, *Hydrological Processes*, 28,
808 4191-4208, 10.1002/hyp.10244, 2014.
- 809 Reggiani, P., Hassanizadeh, S. M., Sivapalan, M., and Gray, W. G.: A unifying framework for
810 watershed thermodynamics: constitutive relationships, *Advances in Water Resources*, 23,
811 15-39, 10.1016/s0309-1708(99)00005-6, 1999.
- 812 Schaefli, B., Hingray, B., Niggli, M., and Musy, A.: A conceptual glacio-hydrological model
813 for high mountainous catchments, *Hydrology and Earth System Sciences*, 9, 95-109,
814 10.5194/hess-9-95-2005, 2005.
- 815 Stadnyk, T. A. and Holmes, T. L.: Large scale hydrologic and tracer aided modelling: A review,
816 *Journal of Hydrology*, 618, 10.1016/j.jhydrol.2023.129177, 2023.
- 817 Su, T., Miao, C. Y., Duan, Q. Y., Gou, J. J., Guo, X. Y., and Zhao, X.: Hydrological response to
818 climate change and human activities in the Three-River Source Region, *Hydrology and
819 Earth System Sciences*, 27, 1477-1492, 10.5194/hess-27-1477-2023, 2023.
- 820 Tang, Q. H., Lan, C., Su, F. G., Liu, X. C., Sun, H., Ding, J., Wang, L., Leng, G. Y., Zhang, Y.
821 Q., Sang, Y. F., Fang, H. Y., Zhang, S. F., Han, D. M., Liu, X. M., He, L., Xu, X. M., Tang,
822 Y., and Chen, D. L.: Streamflow change on the Qinghai-Tibet Plateau and its impacts,
823 *Chinese Science Bulletin-Chinese*, 64, 2807-2821, 10.1360/tb-2019-0141, 2019.
- 824 Tian, F., Hu, H., Lei, Z., and Sivapalan, M.: Extension of the Representative Elementary
825 Watershed approach for cold regions via explicit treatment of energy related processes,
826 *Hydrology and Earth System Sciences*, 10, 619-644, 10.5194/hess-10-619-2006, 2006.
- 827 Tian, F., Xu, R., Nan, Y., Li, K., and He, Z.: Quantification of runoff components in the Yarlung
828 Tsangpo River using a distributed hydrological model, *Advances in Water Science*, 31,
829 324-336, 2020.



- 830 van Pelt, S. C., Kabat, P., ter Maat, H. W., van den Hurk, B., and Weerts, A. H.: Discharge
831 simulations performed with a hydrological model using bias corrected regional climate
832 model input, *Hydrology and Earth System Sciences*, 13, 2387-2397, 10.5194/hess-13-
833 2387-2009, 2009.
- 834 van Pelt, S. C., Kabat, P., ter Maat, H. W., van den Hurk, B. J. J. M., and Weerts, A. H.:
835 Discharge simulations performed with a hydrological model using bias corrected regional
836 climate model input, *Hydrology and Earth System Sciences*, 13, 2387-2397, 10.5194/hess-
837 13-2387-2009, 2009.
- 838 Wang, S., Liu, J., Pritchard, H. D., Ke, L., Qiao, X., Zhang, J., Xiao, W., and Zhou, Y.:
839 Characterizing 4 decades of accelerated glacial mass loss in the west Nyainqentanglha
840 Range of the Tibetan Plateau, *Hydrology and Earth System Sciences*, 27, 933-952,
841 10.5194/hess-27-933-2023, 2023.
- 842 Wang, T., Zhao, Y. T., Xu, C. Y., Ciais, P., Liu, D., Yang, H., Piao, S. L., and Yao, T. D.:
843 Atmospheric dynamic constraints on Tibetan Plateau freshwater under Paris climate
844 targets, *Nature Climate Change*, 11, 10.1038/s41558-020-00974-8, 2021.
- 845 Wang, Y. W., Wang, L., Zhou, J., Yao, T. D., Yang, W., Zhong, X. Y., Liu, R. S., Hu, Z. D., Luo,
846 L., Ye, Q. H., Chen, N. S., and Ding, H. T.: Vanishing Glaciers at Southeast Tibetan Plateau
847 Have Not Offset the Declining Runoff at Yarlung Zangbo, *Geophysical Research Letters*,
848 48, 10.1029/2021gl094651, 2021.
- 849 Wang, L., Han, S., Tian, F., Li, K., Li, Y., Tudaji, M., Cao, X., Nan, Y., Cui, T., Zheng, X., Hu,
850 Z., Wang, W., and Yang, Y.: The Evaporation on the Tibetan Plateau Stops Increasing in
851 the Recent Two Decades, *Journal of Geophysical Research-Atmospheres*, 127,
852 10.1029/2022jd037377, 2022.
- 853 Wang, L., Yao, T. D., Chai, C. H., Cuo, L., Su, F. G., Zhang, F., Yao, Z. J., Zhang, Y. S., Li, X.
854 P., Qi, J., Hu, Z. D., Liu, J. S., and Wang, Y. W.: TP-River: Monitoring and Quantifying
855 Total River Runoff from the Third Pole, *Bulletin of the American Meteorological Society*,
856 102, E948-E965, 10.1175/bams-d-20-0207.1, 2021.
- 857 Wu, Y., Long, D., Lall, U., Scanlon, B. R., Tian, F., Fu, X., Zhao, J., Zhang, J., Wang, H., and
858 Hu, C.: Reconstructed eight-century streamflow in the Tibetan Plateau reveals contrasting
859 regional variability and strong nonstationarity, *Nature Communications*, 13,



- 860 10.1038/s41467-022-34221-9, 2022.
- 861 Xu, R., Hu, H. C., Tian, F. Q., Li, C., and Khan, M. Y. A.: Projected climate change impacts on
862 future streamflow of the Yarlung Tsangpo-Brahmaputra River, *Global and Planetary*
863 *Change*, 175, 144-159, 10.1016/j.gloplacha.2019.01.012, 2019.
- 864 Xu, R., Tian, F., Yang, L., Hu, H., Lu, H., and Hou, A.: Ground validation of GPM IMERG and
865 TRMM 3B42V7 rainfall products over southern Tibetan Plateau based on a high-density
866 rain gauge network, *Journal of Geophysical Research-Atmospheres*, 122, 910-924,
867 10.1002/2016jd025418, 2017.
- 868 Yang, K. and He, J.: China meteorological forcing dataset (1979–2018), National Tibetan
869 Plateau Data Center [dataset], 10.11888/AtmosphericPhysics.tpe.249369.file, 2019.
- 870 Yao, T. D.: Tackling on environmental changes in Tibetan Plateau with focus on water,
871 ecosystem and adaptation, *Science Bulletin*, 64, 417-417, 10.1016/j.scib.2019.03.033,
872 2019.
- 873 Yao, Y. Y., Zheng, C. M., Andrews, C. B., Scanlon, B. R., Kuang, X. X., Zeng, Z. Z., Jeong, S.
874 J., Lancia, M., Wu, Y. P., and Li, G. S.: Role of Groundwater in Sustaining Northern
875 Himalayan Rivers, *Geophysical Research Letters*, 48, 10.1029/2020gl092354, 2021.
- 876 Yao, T. D., Bolch, T., Chen, D. L., Gao, J., Immerzeel, W., Piao, S., Su, F. G., Thompson, L.,
877 Wada, Y., Wang, L., Wang, T., Wu, G. J., Xu, B. Q., Yang, W., Zhang, G. Q., and Zhao, P.:
878 The imbalance of the Asian water tower, *Nature Reviews Earth & Environment*, 3, 618-
879 632, 10.1038/s43017-022-00299-4, 2022.
- 880 Yoshimura, K., Kanamitsu, M., Noone, D., and Oki, T.: Historical isotope simulation using
881 Reanalysis atmospheric data, *Journal of Geophysical Research-Atmospheres*, 113,
882 10.1029/2008jd010074, 2008.
- 883 Zhang, T., Li, D. F., and Lu, X. X.: Response of runoff components to climate change in the
884 source-region of the Yellow River on the Tibetan plateau, *Hydrological Processes*, 36,
885 10.1002/hyp.14633, 2022.
- 886 Zhang, F., Zhang, H. B., Hagen, S. C., Ye, M., Wang, D. B., Gui, D. W., Zeng, C., Tian, L. D.,
887 and Liu, J. S.: Snow cover and runoff modelling in a high mountain catchment with scarce
888 data: effects of temperature and precipitation parameters, *Hydrological Processes*, 29, 52-
889 65, 10.1002/hyp.10125, 2015.



890 Zhao, Q., Ding, Y., Wang, J., Gao, H., Zhang, S., Zhao, C., Xu, J., Han, H., and Shangguan, D.:
891 Projecting climate change impacts on hydrological processes on the Tibetan Plateau with
892 model calibration against the glacier inventory data and observed streamflow, *Journal of*
893 *Hydrology*, 573, 60-81, 10.1016/j.jhydrol.2019.03.043, 2019.